

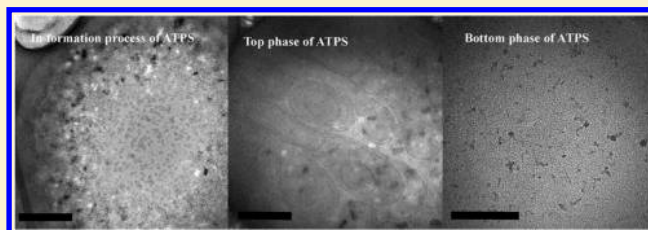
Electrostatic Interactions and Aqueous Two-Phase Separation Modes of Aqueous Mixed Oppositely Charged Surfactants System

Li-Sheng Hao, Yuan-Xiang Gui, Yan-Mei Chen, Shao-Qing He, Yan-Qing Nan,* and Yi-Lan You

College of Chemistry and Chemical Engineering, Hunan Normal University, Changsha 410081, China

S Supporting Information

ABSTRACT: Electrostatic interactions play an important role in setting the aqueous two-phase separation behaviors of mixtures of oppositely charged surfactants. The aqueous mixture of cetyltrimethylammonium bromide (CTAB) and sodium dodecylsulfonate (AS) is actually a five-component system, comprised of CTAB, AS, complex salt (cetyltrimethylammonium dodecylsulfonate, abbreviated as CTA^+AS^-), NaBr, and water. In the three-dimensional pyramid phase diagram, the aqueous two-phase region with excess AS or with excess CTAB extends successively from the region very near to the NaBr–H₂O line through the CTAB–AS–H₂O conventional mixing plane to the CTA^+AS^- –AS–H₂O side plane or to the CTA^+AS^- –CTAB–H₂O side plane, respectively. Large or small molar ratios between the counterions and their corresponding surfactant ions for oppositely charged surfactants located in the NaBr side or the CTA^+AS^- side of the pyramid imply strong or weak electrostatic screening. Electrostatic screening of counterions alters the electrostatic attractions between the oppositely charged head groups or the electrostatic repulsions between the like-charged head groups in excess, and the electrostatic free energy of aggregation thus affects the aqueous two-phase separation modes. Composition analysis, rheological property investigation, and TEM images suggest that there are two kinds of aqueous two-phase systems (ATPSs). On the basis of these experimental results and Kaler's cell model, two kinds of phase separation modes were proposed. Experimental results also indicate that all of the top phases are surfactant-rich, and all of the bottom phases are surfactant-poor; the density difference between the top phase and the bottom phase in one ATPS is very small; the interfacial tension (σ) of the ATPS is ultralow.



1. INTRODUCTION

Aqueous mixtures of oppositely charged surfactants exhibit interesting properties and phase behaviors that are largely a result of strong electrostatic attractions between oppositely charged head groups.^{1–34} Aqueous two-phase separation phenomena of cationic/anionic surfactants^{30–41} have attracted considerable attention due to the potential application to the isolation and purification of biomaterials while maintaining their bioactivity. Previous research revealed that the aqueous two-phase separation behavior is closely related to the microstructures of the aggregates as well as the interactions between the aggregates. Aqueous two-phase separation may occur due to the entanglement of rod-like micelles, the formation of a lamellar phase, or the formation of densely packed vesicles.³⁷

It is well-known that electrostatic interactions play a prominent role in setting the molecular self-assemblies³³ and the phase behaviors⁴² of aqueous mixtures of oppositely charged surfactants. Both inter- and intra-aggregate electrostatic interactions are important in setting the stability of all charged amphiphile assemblies. The addition of inorganic salt into the aqueous mixtures of oppositely charged surfactants increases the concentration of inorganic counterions and thus increases the electrostatic screening of the intra-aggregate electrostatic repulsion between the like-charged head groups in excess, the

intra-aggregate electrostatic attraction between the oppositely charged head groups, and the interaggregate electrostatic repulsion, therefore influencing the shape, size, and composition of the aggregates formed and changing the phase behaviors. For samples containing 2 wt % 21/79 (molar ratio) CTAB/SOS, experiments of Kaler's group^{42,43} illustrate that thermodynamically stable unilamellar vesicles with an apparent radius of approximately 130 nm and a much more equimolar composition (CTAB/SOS of molar ratio 45/55) than the bulk composition form in the absence of salt; SANS experiments indicate that vesicles coexist with elongated micelles in the 0.5 wt % NaBr aqueous solution; the phase separates at intermediate NaBr concentrations between 1.4 and 2.5 wt %; micelles not purely spherical but somewhat elongated in an ellipsoidal or cylindrical shape with an apparent radius of approximately 10 nm and a composition equal to the bulk composition form at a high salt concentration (5.0 wt % NaBr). These investigations suggest that weak electrostatic screening that originated from the constituent counterions of the surfactant in the absence of salt is beneficial for the formation of aggregates that are more equimolar in composition than the

Received: April 17, 2012

Revised: July 15, 2012

Published: August 1, 2012

bulk mixing ratio, while strong electrostatic screening coming from the added salt is beneficial for the formation of aggregates with compositions approaching that of the bulk.

Kaler's group^{2,42,43} has developed a statistical thermodynamic cell model and has used the model to calculate the optimum composition of aggregates as a function of added salt and to interpret the experimental data. Of all of the contributions to the total free energy of aggregation, only the electrostatic free energy G_{el} is sensitive to electrolyte concentration. With no added salt, G_{el} is relatively high and thus favors a more electroneutral aggregate. Upon addition of salt, the increased counterions shield the charged aggregates and reduce G_{el} for a given aggregate composition. At high concentrations of added salt, the aggregate composition approaches that of the bulk. Blankschtein's group⁴⁴ has developed a molecular thermodynamic theory to describe the formation of cationic/anionic vesicles. The composition in cationic/anionic vesicles is partly controlled by the electrostatic free energy, which, in turn, depends on the ionic strength of the solution. At low ionic strengths, the electrostatic free energy is so strong that deviations from a nearly equimolar cationic/anionic surfactant mixture in the vesicle would result in a large free-energy penalty; thus, the vesicle composition would remain close to that of an equimolar mixture. As the ionic strength increases, however, the importance of the electrostatic free energy diminishes; the composition of the vesicle would reflect the difference in monomeric surfactant concentrations, and thus, the vesicle composition deviates from equimolar further and progressively approaches that of the bulk.

Furthermore, inorganic-salt-induced rod-like micelle-to-vesicle transition in aqueous solutions composed of DTAB and an excess of SDS,^{7,45} inorganic-salt-induced aqueous two-phase separation in aqueous mixed systems composed of gemini surfactant 12-3-12 and an excess of AS,⁴⁶ and inorganic-salt-induced phase inversion of the ATPS in aqueous mixed systems composed of AS and an excess of 12-3-12³⁹ also clearly demonstrate the importance of electrostatic interactions in setting microstructures of aggregates and the phase behaviors of cationic/anionic surfactants.

Aqueous mixtures of cationic (A^+X^-) and anionic surfactants (A^-X^+) are actually five-component systems in the sense of Gibbs phase rule:^{18,47} A^+X^- , A^-X^+ , A^+A^- (complex salt or ion pair amphiphile), X^+X^- (simple salt), and water. The electroneutrality condition reduces the number of independent components to four. The full phase diagram should be represented in three dimensions such as the pyramid-shaped diagram.⁴⁸ Ionic composition analysis confirms that aqueous two-phase separating samples in the conventional mixing plane do not in general give constituent phases in that plane.^{40,41,49,50} Therefore, to represent the liquid–liquid phase equilibrium of ATPSs, three-dimensional phase diagrams are needed.

Although many reports^{30–41,46,49,50} involve aqueous two-phase separation phenomena, systematic investigations on the phase separation mechanism are still desired.³⁷ For the $A^+X^-/A^-X^+/A^+A^-/X^+X^-/H_2O$ mixed systems in the different position of the pyramid phase diagram, the molar ratios between the surfactant ions and their counterions are variable. These variations may modify both inter- and intra-aggregate electrostatic interactions, thus influencing aggregation behavior and phase behavior. For the aqueous mixed cationic surfactant A^+X^- /anionic surfactant A^-X^+ system, the addition of simple salt X^+X^- increases the molar ratio between counterions and their corresponding surfactant ions, thus reinforcing the

electrostatic screening effect due to the counterion binding. On the contrary, the elimination of parts of the inorganic ions, or the addition of the complex salt A^+A^- , increases the molar ratio between surfactant ions and their counterions, thus weakening the electrostatic screening effect; however, will the aqueous two-phase separation phenomena still be observed? If one kind of inorganic ion was eliminated totally from the mixed systems, the remaining mixed system, that is, the $A^+X^-/A^+A^-/H_2O$ or $A^-X^+/A^+A^-/H_2O$ mixed system, will be a truly ternary mixed system; then, what kind of phase behavior will be observed? Will the properties of the ATPSs and aqueous two-phase separation modes change with the variation of the molar ratios between the surfactant ions and their counterions? In order to answer the aforementioned questions, the extension of aqueous two-phase regions in three-dimensional space, the microstructures, compositions, and properties of the coexisting phases in ATPSs located at different spaces of a pyramid phase diagram need to be investigated. This systematic research is necessary for a fundamental understanding of the aqueous two-phase separation and also for the development of theoretical models for the prediction of the partitioning behavior of the ATPS.

In this paper, the aqueous two-phase behaviors for the CTAB/AS/CTA⁺AS[−]/NaBr/H₂O system at 318.15 K have been investigated. To investigate the electrostatic interaction effect on aqueous two-phase separation behaviors, the pyramid phase diagram of ATPSs formed by the mixed system has been drawn. Eleven representative ATPSs in different positions of the pyramid phase diagram were chosen for composition analysis, density and interfacial tension measurement, rheological experiment, and microstructure observation. Kaler's cell model has been used to interpret the aqueous two-phase separation modes.

2. THEORY

2.1. Coulomb's law. Generally, the electrostatic interaction between electrically charged particles is described by Coulomb's law

$$F = \frac{q_1 q_2}{4\pi\epsilon\epsilon_0 r^2} \quad (1)$$

where F is the electrostatic force, q_1 and q_2 are the magnitudes of the charges, r is the separation distance, ϵ is dielectric constant of the medium, and ϵ_0 is the permittivity of vacuum. Like charges repel each other; opposite charges attract each other.

For aqueous mixed cationic and anionic surfactant systems, addition of inorganic salt usually leads to a certain decrease of ϵ ;⁵¹ meanwhile, the increase of the amounts of inorganic ions results in stronger counterion binding with charged aggregates, thus causing the decrease of the effective magnitude of charge for the ionic head groups. Therefore, for two ionic head groups or two charged aggregates with a certain separation distance r , the decrease of ϵ favors the electrostatic interaction, whereas the counterion binding depresses the electrostatic interaction; the overall result is the depression of the electrostatic interaction. The addition of inorganic salt into aqueous mixed cationic and anionic surfactant systems weakens the electrostatic attraction between the oppositely charged head groups, the electrostatic repulsion between the like-charged head groups, and the interaggregate electrostatic repulsion.

2.2. Cell Model. Kaler's group^{2,42,43} proposed a method to describe the Gibbs free energy of a mixed micellar solution of cationic and anionic surfactants within the framework of a thermodynamic cell model. A solution of given composition is divided into cells, each cell containing one aggregate. The aggregates are assumed to be noninteracting, which is justified by the small Debye length relative to the aggregate size over the concentration range of interest. They indicated that phase behavior and optimal aggregate properties are calculated by directly minimizing the Gibbs free energy, rather than by equating chemical potentials of each phase. The total free energy of aggregation is given by

$$G_{\text{agg}} = \sum n_i \mu_i^{\ominus, \text{W}} + \Delta G_{\text{agg}} \quad (2)$$

Here, n_i is the number of molecules of species i in the cell, $\mu_i^{\ominus, \text{W}}$ is the standard chemical potential of species i in water, and the summation is over components i in the aqueous region of the cell.

For micelles or aggregates, the free-energy change is calculated by summing the contributions favoring and opposing aggregation

$$\Delta G_{\text{agg}} = G_{\text{hyd}} + G_{\text{mic}} + G_{\text{mix}} + G_{\text{el}} + G_{\text{int}} + G_{\text{ch}} + G_{\text{id}} + G_{\text{st}} \quad (3)$$

The hydrophobic tail transfer free energy G_{hyd} favors aggregation. The α -methylene group (next to the head group) is assumed to protrude into the water.⁴³ Thus, G_{hyd} is approximated by the relation

$$G_{\text{hyd}} = A + B(n_{\text{C}} - 1) \quad (4)$$

where n_{C} is the number of carbons in the surfactant tail. The ideal entropy of mixing a micelle with other molecules in the cell, G_{mic} , and the ideal entropy of mixing surfactant ions within a mixed micelle, G_{mix} , also favor aggregation. These contributions are balanced against those opposing aggregation: the electrostatic free-energy contribution to aggregation G_{el} , the interfacial free energy G_{int} , which represents the penalty for establishing a water/hydrocarbon interface, the free-energy contribution for the hydrophobic tail chain packing within the micelle G_{ch} (the formalism of Szleifer's mean-field model^{52,53} is used), the free-energy contribution arising from steric interactions between head groups G_{st} , and the ideal entropy of mixing G_{id} in the aqueous region containing water, monomeric surfactant, and counterions. The formalisms of these Gibbs free-energy contributions refer to refs 2, 42, and 43.

The electrostatic free-energy contribution to aggregation G_{el} was calculated by first numerically solving the nonlinear Poisson–Boltzmann equation (PBE), which in spherical coordinates is given by

$$\begin{aligned} \nabla^2 \psi(r) &= \frac{d^2 \psi}{dr^2} + \frac{2}{r} \frac{d\psi}{dr} \\ &= -\frac{\rho(r)}{\epsilon_0 \epsilon} \\ &= -\sum \frac{z_i e \rho_i^\infty}{\epsilon_0 \epsilon} \exp(-z_i e \psi / k_{\text{B}} T) \end{aligned} \quad (5)$$

where ψ is the electrostatic potential and $\rho(r)$ is the charge density at r . Solution of the PBE is subject to mass balance constraints over all of the aqueous ionic species. The nonlinear

PBE was solved numerically for each trial of parameters in the cell model free-energy minimization, which satisfied the corresponding boundary conditions, followed by numerical integration over the potential distribution to calculate the enthalpic and entropic contributions to the electrostatic free energy.^{2,42} Thus, the exact potential and electrostatic free energy G_{el} can be obtained. For example, for spherical micelles, G_{el} is

$$G_{\text{el}} = \frac{1}{2} \psi_s N_{\text{agg}} e \sum_{i=1}^2 z_i \alpha_i + \frac{L e}{2} \int_{R_1}^{R_2} \sum_{i=1}^q z_i c_i(r) \psi(r) 4\pi r^2 dr \quad (6)$$

where ψ_s is the potential at the micellar surface, α_i is the mole fraction of surfactant ion i in the mixed micelle, N_{agg} is the aggregation number of the micelle, L is Avogadro's constant, the sum q is over counterions and monomeric surfactant ions, and z_i and $c_i(r)$ are the electrovalency and the local concentration of ion i , respectively. For the rod-like or lamellar aggregates or vesicles,^{42,43} there are similar terms as those in eq 6 when calculating G_{el} . Equation 6 tells us that the decreases of surface charge $e \sum_{i=1}^2 z_i \alpha_i$, the surface potential ψ_s , and the thickness of the electrical double layer reduce G_{el} effectively. That is why in the sample containing 2.0 wt % 21/79 (molar ratio) CTAB/SOS in the absence of inorganic salt, the composition of the formed vesicles is much more nearly equimolar than the bulk mixing ratio.

3. EXPERIMENTAL SECTION

3.1. Materials. Sodium dodecylsulfonate (AS) (purity $\geq 97\%$) was recrystallized as previously.^{39–41} Cetyltrimethylammonium bromide (CTAB) purchased from Sinopharm Chemical Reagent Co., Ltd. (purity $\geq 99\%$) was used without further purification. Complex salts (CTA^+AS^-) were synthesized by the direct mixture of equimolar solutions of the AS and CTAB, according to the literature method.^{54,55} The precipitate of complex salt was washed several times with redistilled water to remove the resulting NaBr and traces of coprecipitated ionic surfactant. Sodium bromide (NaBr), AR, was purchased from Shanghai No. 4 Reagent Factory. All of the solid samples were dried in a vacuum desiccator at 333.15 K for 24 h before use. Water was redistilled from potassium permanganate solution.

3.2. Sample Preparations. For the samples in the conventional mixing plane (i.e., CTAB–AS–H₂O plane) or in the sections located on the NaBr side of the pyramid phase diagram, surfactant stock solutions were prepared by dissolving weighed amounts of AS or CTAB in pure water or NaBr aqueous solution; the samples were prepared by mixing stock solutions of AS and CTAB with the same mole fraction x at the desired ratio in 5 mL test tubes with a graduation interval of 0.1 mL. The total mole fraction x_{T} of surfactant and NaBr equaled $1 - x_{\text{water}}$ and the mole fraction of surfactant stock solutions x was $1 - x_{\text{NaBr}} - x_{\text{water}}$ for the samples in the conventional mixing plane, $x_{\text{NaBr}} = 0$.

For the samples in the CTAB–CTA⁺AS[−]–H₂O or AS–CTA⁺AS[−]–H₂O side plane, or samples lying in the sections located on the CTA⁺AS[−] side of pyramid phase diagram, for each desired total mole fraction x_{T} of surfactant and complex salt equal to $1 - x_{\text{water}}$, weighed amounts of CTA⁺AS[−] and water were added into the test tubes according to the molar ratio x_{T} , $(1 - x_{\text{T}})$; then, a weighed amount of CTAB or (and) AS aqueous solution with x_{T} was added into the test tube to the desired ratio and mixed with CTA⁺AS[−] and water.

For phase behavior experiments, phase instability and supersaturated phenomena should be excluded.⁵⁶ Some steps were adopted to ensure that the equilibrated phase behaviors of the samples were observed. (1) The weighing process was performed at room temperature; thus, the temperature of the originally prepared samples was close to room temperature. (2) Then, all of the samples were mixed thoroughly in the test tubes. The test tubes were immersed in a water bath at 318.15 ± 0.01 K for about 100 h or longer until an equilibrium state was attained. (3) In order to verify the equilibrium state of the samples, some of the samples were kept at 318.15 ± 0.01 K for a longer time, such as a month; the observed phase behaviors remained unchanged; some of the samples in the equilibrium state were cooled at room temperature for several hours, white precipitates were observed, and then, the test tubes with these samples were immersed in a water bath at 318.15 ± 0.01 K again, and the original equilibrated phase behaviors were recovered. The phase behavior experiments were performed within $0.001 \leq x_T \leq 0.010$ and were based on about 2000 samples.

3.3. Composition Measurements. According to our previous work,^{39–41,50} first, a certain amount of solution of the top phase or the bottom phase of an ATPS was weighed and then was kept at 323.15 ± 0.1 K in a water bath for about 1 or 2 days, until the water in the solution was evaporated thoroughly. The solid substance obtained was mixed thoroughly and dried in a vacuum desiccator at 323.15 K for 24 h and then was weighed and analyzed by an elementary analyzer (Elementar Analysensysteme GmbH VarioEL CHNS mode) made in Germany. The amounts of CTA^+ and AS^- in a sample were obtained directly by the amounts of elemental nitrogen, sulfur, and carbon. The amounts of Na^+ and Br^- were calculated by the material balance equation and the electro-neutrality equation.

For the ATPS with NaBr aqueous solution as the solvent, or the ATPS–C with pure water as the solvent and with two separating isotropic phases, the concentrations of the surfactant AS and CTAB in the dilute bottom phases of ATPSs were very low (about several dozen $\mu\text{mol}\cdot\text{kg}^{-1}$); these dilute phases were almost NaBr aqueous solutions. The concentrations of the Br^- ions were determined by the Mohr method. The Mohr method uses potassium chromate as an indicator in the titration of bromide ions with a silver nitrate standard solution. After all of the bromide ions have been precipitated, the first excess of titrant results in formation of a brick-red silver chromate precipitate, which signals the end point. For standard solutions, the measurement error of the Mohr method is usually less than 0.5%.

3.4. Viscosity Measurements. Shear viscosities of the separated phases in ATPSs were measured using a Brookfield Cone and Plate Viscometer Model (RVDV-III Ultra programmable rheometer) with a CP40 spindle at 318.15 ± 0.1 K.

3.5. Phase Density Measurements. The densities of separated phases in ATPSs were determined using a 10 mL density bottle and a 0.1 mg balance. The measurements were performed at 318.15 ± 0.1 K.

3.6. Interfacial Tension Measurements. The interfacial tensions of ATPSs were determined by the spinning drop interface tensiometer (TX500D, USA KINO Industry Co., Ltd.). The capillary tube was filled with the higher density liquid, and the drop was made with a lower density liquid. The tube was then spun at different speeds in such a way that the

droplet inside of the tube was elongated to exceed four times the diameter.

3.7. Polarization Microscopy. The liquid-crystalline phase was judged by visual inspection between crossed polarizers. Photographs of birefringence were taken by optical microscopy with crossed polarizers (Nikon, China, YS2-H).

3.8. Electron Microscopy. Cryo-TEM samples were prepared in a controlled environment vitrification system (CEVS) at 298.15 K. A micropipet was used to load 5 μL of solution onto a TEM copper grid, which was blotted with two pieces of filter paper, resulting in the formation of thin films suspended on the mesh holes. After waiting for about 5 s, the samples were quickly plunged into a reservoir of liquid ethane (cooled by the liquid nitrogen) at -165 °C. The vitrified samples were then stored in the liquid nitrogen until they were transferred to a cryogenic sample holder (Gatan 626) and examined with a JEOL JEM-1400 (120 kV) at about -174 °C. The phase contrast was enhanced by underfocus. The images were recorded on a Gatan multiscan CCD and processed with a digital micrograph.

Negative stained electron micrographs were obtained as previously described.⁵⁷

4. RESULTS AND DISCUSSION

4.1. Pyramid Phase Diagram of Aqueous Two-Phase Regions. The phase behaviors of the samples with $0.001 \leq x_T \leq 0.010$ located at different positions of the pyramid phase diagram have been investigated at 318.15 K. In the pyramid, water (H_2O) is placed at the top, and the four corners of the base are AS, NaBr, CTAB, and CTA^+AS^- with a mole fraction of $x_T = 0.010$ in a clockwise sequence. Phase behavior investigations are based on the following chosen planes and sections of the pyramid: conventional CTAB–AS– H_2O mixing plane, CTAB– CTA^+AS^- – H_2O side plane, AS– CTA^+AS^- – H_2O side plane, four sections between the conventional mixing plane and the CTAB– CTA^+AS^- – H_2O side plane, four sections between the conventional mixing plane and the AS– CTA^+AS^- – H_2O side plane, and three sections parallel to the base of the pyramid on the NaBr side. Analogous to the case in the conventional mixing plane,⁴⁰ seven phase regions are divided according to the macrophase behaviors in the pyramid phase diagram. Figure 1 presents the phase diagrams in the conventional CTAB–AS– H_2O mixing plane of the pyramid. Phase regions 2 and 6 are aqueous two-phase regions with anionic or cationic surfactant in excess, named the ATPS-A

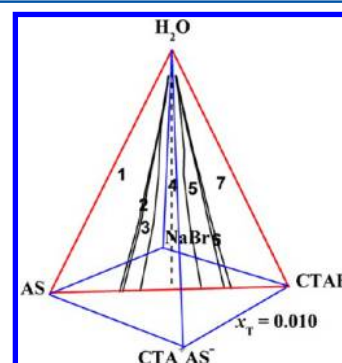


Figure 1. The conventional mixing plane in the pyramid phase diagram. Red triangle: the chosen plane being investigated. Black curves: the phase boundaries in the chosen plane. Dashed line: the equimolar line.

region and ATPS-C region, respectively. Each ATPS region is surrounded by one isotropic single-phase region and one lamellar liquid-crystalline phase region. Phase regions 1 and 7 are isotropic single-phase regions, located at the left side of the ATPS-A region or the right side of the ATPS-C region, in which rod-like micelles usually form.^{57,58} Lamellar liquid-crystalline phase regions 3 or 5 are located at the other side of the ATPS-A or ATPS-C region, respectively. Phase region 4 is a heterogeneous phase region that is located between phase regions 3 and 5; usually the precipitate coexists with a liquid phase.

Three kinds of representative optical phenomena were observed for the aqueous two-phase systems. (1) A birefringent top phase with textures of lamellar liquid crystals coexists with an isotropic bottom phase. (2) An isotropic top phase coexists with a birefringent bottom phase. (3) Both the top and the bottom phases are isotropic.

Experimental results illustrate that the seven phase regions extend successively in the three-dimensional space of the pyramid phase diagram. Because of theoretical interest and potential applications for the separation and purification of biological macromolecules, we pay special attention to ATPS regions. The pyramid phase diagrams of the ATPS-A and ATPS-C regions are depicted in Figure 2. The three-

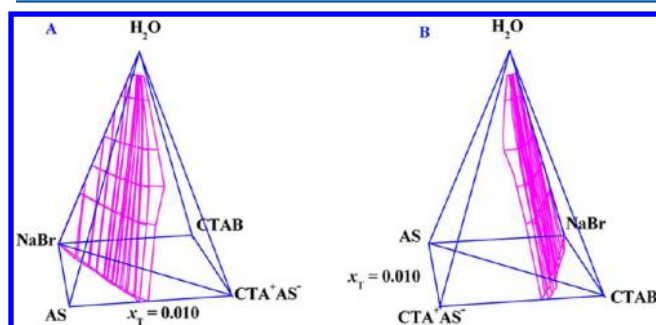


Figure 2. The pyramid phase diagrams of the ATPS-A region and ATPS-C region. (A) ATPS-A region; (B) ATPS-C region.

dimensional bodies with magenta color represent the ATPS-A and ATPS-C regions, respectively. ATPS-A region and ATPS-C region extend successively from the region very near to the NaBr–H₂O line through the conventional mixing plane to the CTA⁺AS[−]–AS–H₂O side plane and the CTA⁺AS[−]–CTAB–H₂O side plane, respectively. The ATPS regions are very narrow in the three-dimensional space, illustrating that this kind of phase separation only occurs under a certain molar ratio range of the two oppositely charged surfactant ions. Experimental results also indicate that under certain x_T , both ATPS-A region and ATPS-C region shift to spaces far away from the equimolar composition of AS[−] and CTA⁺ with the increase of the counterions. The increase of x_T has a similar influence on phase boundaries of ATPS regions. These phenomena are closely related to the counterion electrostatic screening effect on the aggregate formation and the interactions between the aggregates.⁴⁶

4.2. Ionic Compositions of the Separated Phases in ATPSs. Ionic composition analysis can reveal the concentrations of CTA⁺, AS[−], Na⁺, and Br[−] ions in the separated phases of ATPSs, which can be used to interpret the properties and extraction efficiency of ATPSs. Eleven representative ATPSs located at different positions on the pyramid phase diagram were chosen for ionic composition analysis to

investigate the influence of electrostatic interaction on the compositions of the separated phases in one ATPS. The results are presented in Table 1.

All of the top phases in ATPS are surfactant-rich, and all of the bottom phases are surfactant-poor. In comparison with the top phases, the molar ratios between the counterions and their corresponding surfactant ions in the bottom phases are larger. The phase separation process is analogous to that of oppositely charged polyelectrolyte/surfactant aqueous mixed systems^{59–61} at a certain degree, it involves an ion exchange process: the surfactant ions in the concentrated phase lost some of their original counterions and acquired some oppositely charged surfactant ions in exchange, that is, in the concentrated phase, and for the aggregates formed by oppositely charged surfactant ions, some of their original counterions were released to the dilute phase. This means that all of the tie lines of ATPS have the same orientation as described by Figure 3: the bottom phases orientate to the NaBr side, and the top phases orientate to the CTA⁺AS[−] side.

For the ATPSs located at the NaBr side of the pyramid phase diagram, typical phase behaviors are analogous to samples *n*1–*n*4; their tie lines are located at the NaBr side of the pyramid. For those ATPSs located in or near the conventional mixing plane, typical phase behaviors are analogous to samples *n*5–*n*7; these tie lines stride across the conventional mixing plane from the NaBr side to the CTA⁺AS[−] side. For those ATPSs located at the CTA⁺AS[−] side of the pyramid, the typical phase behaviors are analogous to samples *n*8 and *n*9; their tie lines locate at the CTA⁺AS[−] side. For the ATPS-A located on the CTA⁺AS[−]–AS–H₂O side plane, the typical phase behavior of the ATPS-A is analogous to that of sample *n*10; as true ternary systems due to the absence of the inorganic Br[−] counterions, their tie lines lie on the CTA⁺AS[−]–AS–H₂O side plane. Analogously, the typical phase behavior of ATPS-C located in the CTA⁺AS[−]–CTAB–H₂O side plane is analogous to sample *n*11; their tie lines lie on the CTA⁺AS[−]–CTAB–H₂O side plane.

The composition analysis results suggest that there are two kinds of ATPSs. ATPSs at the NaBr side similar to samples *n*1–*n*4 belong to the first kind of ATPS; almost all of the surfactant ions are concentrated to the top phases, and the molar ratio of CTA⁺ to AS[−] (MR_{CTA^+/AS^-}) in the top phase is equal to that in the whole ATPS; the concentrations of surfactant ions in the bottom phases are very dilute, almost close to the critical micelle concentration (CMC) of this cationic/anionic surfactant system. ATPSs at the CTA⁺AS[−] side similar to samples *n*8–*n*11 belong to the second kind of ATPS; the concentration differences of surfactant ions between the top phases and the corresponding bottom phases are small. MR_{CTA^+/AS^-} in the top phase, MR_{CTA^+/AS^-} in the corresponding bottom phase, and MR_{CTA^+/AS^-} in the whole ATPS are different from each other. For ATPSs located in or near the conventional mixing plane, both of the above kinds of ATPSs were observed. ATPS-C with two isotropic coexisting phases similar to that of sample *n*7 belongs to the first kind of ATPS. The other ATPSs with one birefringent phase and one isotropic phase similar to those of samples *n*5 and *n*6 belong to the second kind of ATPS.

Usually, ions can be classified as being either kosmotropes or chaotropes according to their relative abilities to alter the structure of surrounding water molecules. Following Collins's concept of matching water affinities,^{7,58,62,63} the tendency of oppositely charged ions spontaneously associating as inner-

Table 1. Ionic compositions of the Separated Phases in Some ATPSs

| sample number | composition | top phase 1000x | bottom phase 1000x | ATPS (measured) 1000x | ATPS (prepared) 1000x | error (%) |
|---|--|--------------------|-----------------------|--------------------------|--------------------------|--------------|
| <i>n</i> 1 | Optical Property | Isotropic | Isotropic | | | |
| (ATPS-A) NaBr side of pyramid | CTA ⁺ | 1.096 | 0.00037 | 0.577 | 0.558 | 3.41 |
| | AS [−] | 2.403 | 0.00080 | 1.266 | 1.255 | 0.88 |
| | Br [−] | 2.256 | 2.479 | 2.362 | 2.354 | 0.34 |
| | Na ⁺ | 3.564 | 2.479 | 3.050 | 3.051 | −0.03 |
| | MR _{CTA⁺/AS[−]} | 0.456 | 0.462 | 0.456 | 0.445 | 2.47 |
| | total | 4.660 | 2.480 | 3.628 | 3.609 | 0.53 |
| <i>n</i> 2 | Optical Property | Birefringent | Isotropic | | | |
| (ATPS-A) NaBr side of pyramid | CTA ⁺ | 1.640 | 0.00038 | 0.596 | 0.578 | 3.11 |
| | AS [−] | 3.369 | 0.00079 | 1.225 | 1.235 | −0.81 |
| | Br [−] | 2.175 | 2.522 | 2.396 | 2.374 | 0.93 |
| | Na ⁺ | 3.905 | 2.522 | 3.025 | 3.031 | −0.20 |
| | MR _{CTA⁺/AS[−]} | 0.487 | 0.481 | 0.487 | 0.468 | 4.06 |
| | total | 5.544 | 2.523 | 3.621 | 3.609 | 0.33 |
| <i>n</i> 3 | Optical Property | Birefringent | Isotropic | | | |
| (ATPS-C) NaBr side of pyramid | CTA ⁺ | 4.663 | 0.00085 | 1.367 | 1.316 | 3.88 |
| | AS [−] | 1.754 | 0.00032 | 0.514 | 0.497 | 3.42 |
| | Br [−] | 4.947 | 2.383 | 3.135 | 3.112 | 0.74 |
| | Na ⁺ | 2.039 | 2.383 | 2.282 | 2.293 | −0.44 |
| | MR _{CTA⁺/AS[−]} | 2.658 | 2.656 | 2.660 | 2.647 | 0.46 |
| | total | 6.701 | 2.384 | 3.649 | 3.609 | 1.11 |
| <i>n</i> 4 | Optical Property | Isotropic | Isotropic | | | |
| (ATPS-C) NaBr side of pyramid | CTA ⁺ | 3.455 | 0.00088 | 1.351 | 1.357 | −0.37 |
| | AS [−] | 1.211 | 0.00031 | 0.474 | 0.456 | 3.95 |
| | Br [−] | 4.358 | 2.351 | 3.136 | 3.153 | −0.54 |
| | Na ⁺ | 2.115 | 2.351 | 2.259 | 2.252 | 0.31 |
| | MR _{CTA⁺/AS[−]} | 2.853 | 2.839 | 2.850 | 2.976 | −4.23 |
| | total | 5.569 | 2.352 | 3.610 | 3.609 | 0.03 |
| <i>n</i> 5 | Optical Property | Birefringent | Isotropic | | | |
| (ATPS-A) Conventional Mixing plane | CTA ⁺ | 0.836 | 0.576 | 0.648 | 0.648 | 0 |
| | AS [−] | 1.475 | 1.045 | 1.164 | 1.151 | 1.13 |
| | Br [−] | 0.647 | 0.651 | 0.649 | 0.648 | 0.15 |
| | Na ⁺ | 1.286 | 1.121 | 1.166 | 1.151 | 1.30 |
| | MR _{CTA⁺/AS[−]} | 0.567 | 0.551 | 0.557 | 0.562 | −0.89 |
| | total | 2.122 | 1.696 | 1.813 | 1.799 | 0.78 |
| <i>n</i> 6 | Optical Property | Isotropic | Birefringent | | | |
| (ATPS-C) Conventional Mixing plane | CTA ⁺ | 1.627 | 0.905 | 1.200 | 1.225 | −2.04 |
| | AS [−] | 0.725 | 0.432 | 0.550 | 0.574 | −4.18 |
| | Br [−] | 1.462 | 1.056 | 1.223 | 1.225 | −0.16 |
| | Na ⁺ | 0.559 | 0.583 | 0.574 | 0.574 | 0 |
| | MR _{CTA⁺/AS[−]} | 2.244 | 2.095 | 2.182 | 2.134 | 2.24 |
| | total | 2.186 | 1.488 | 1.774 | 1.799 | −1.39 |
| <i>n</i> 7 | Optical Property | Isotropic | Isotropic | | | |
| (ATPS-C) conventional mixing plane | CTA ⁺ | 1.642 | 0.00080 | 1.239 | 1.229 | 0.81 |
| | AS [−] | 0.753 | 0.00037 | 0.569 | 0.570 | −0.18 |
| | Br [−] | 1.422 | 0.668 | 1.237 | 1.229 | 0.65 |
| | Na ⁺ | 0.534 | 0.668 | 0.567 | 0.570 | −0.53 |
| | MR _{CTA⁺/AS[−]} | 2.181 | 2.162 | 2.178 | 2.156 | 1.01 |
| | total | 2.176 | 0.669 | 1.806 | 1.799 | 0.39 |
| <i>n</i> 8 | Optical Property | Birefringent | Isotropic | | | |
| (ATPS-A) CTA ⁺ AS [−] side of pyramid | CTA ⁺ | 1.298 | 0.473 | 0.813 | 0.793 | 2.52 |
| | AS [−] | 1.947 | 0.862 | 1.310 | 1.324 | −1.06 |
| | Br [−] | 0.500 | 0.470 | 0.482 | 0.475 | 1.47 |
| | Na ⁺ | 1.149 | 0.858 | 0.979 | 1.006 | −2.68 |
| | MR _{CTA⁺/AS[−]} | 0.667 | 0.549 | 0.621 | 0.599 | 3.68 |
| | total | 2.447 | 1.332 | 1.792 | 1.799 | −0.39 |
| <i>n</i> 9 | Optical Property | Birefringent | Isotropic | | | |
| (ATPS-A) CTA ⁺ AS [−] side of pyramid | CTA ⁺ | 1.698 | 0.527 | 0.889 | 0.914 | −2.74 |
| | AS [−] | 2.571 | 0.927 | 1.434 | 1.477 | −2.91 |
| | Br [−] | 0.255 | 0.362 | 0.329 | 0.322 | 2.17 |

Table 1. continued

| sample number | composition | top phase 1000x | bottom phase 1000x | ATPS (measured) 1000x | ATPS (prepared) 1000x | error (%) |
|--|--|--------------------|-----------------------|--------------------------|--------------------------|--------------|
| n9 | Optical Property | Birefringent | Isotropic | | | |
| | Na ⁺ | 1.128 | 0.761 | 0.874 | 0.885 | −1.24 |
| | MR _{CTA⁺/AS[−]} | 0.660 | 0.569 | 0.620 | 0.619 | 0.16 |
| | total | 2.827 | 1.289 | 1.763 | 1.799 | −2.00 |
| n10 (ATPS-A) CTA ⁺ AS [−] –AS–H ₂ O side plane | Optical Property | Birefringent | Isotropic | | | |
| | CTA ⁺ | 4.049 | 1.635 | 2.619 | 2.674 | −2.06 |
| | AS [−] | 5.769 | 2.749 | 4.004 | 4.000 | 0.10 |
| | Br [−] | 0 | 0 | 0 | 0 | |
| | Na ⁺ | 1.720 | 1.114 | 1.386 | 1.326 | 4.52 |
| | MR _{CTA⁺/AS[−]} | 0.702 | 0.595 | 0.654 | 0.669 | −2.17 |
| | total | 5.769 | 2.749 | 4.004 | 4.000 | 0.13 |
| n11 (ATPS-C) CTA ⁺ AS [−] –CTAB–H ₂ O side plane | Optical Property | Birefringent | Isotropic | | | |
| | CTA ⁺ | 3.893 | 1.836 | 3.052 | 3.000 | 1.73 |
| | AS [−] | 2.673 | 1.072 | 2.017 | 2.023 | −0.30 |
| | Br [−] | 1.221 | 0.764 | 1.035 | 0.977 | 5.94 |
| | Na ⁺ | 0 | 0 | 0 | 0 | – |
| | MR _{CTA⁺/AS[−]} | 1.456 | 1.713 | 1.513 | 1.483 | 2.03 |
| | total | 3.893 | 1.836 | 3.052 | 3.000 | 1.73 |

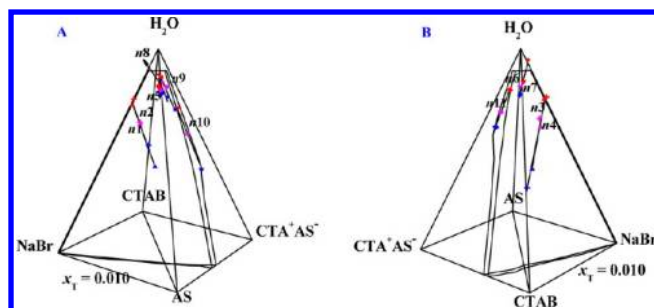


Figure 3. Tie lines of some ATPS-A and ATPS-C. (A) ATPS-A; (B) ATPS-C.

sphere ion pairs in aqueous solution is relative to matching absolute free energies of ion hydration. This is supposed to be due to the fact that the strength of interaction between the ions and the water molecules is correlated to the strength with which the ion interacts with other ions. Chaotropic counterions (e.g., Br[−]) can form direct ion pairs with chaotropic ionic head groups (e.g., the head group of CTA⁺), much like kosmotropic counterions with kosmotropic ionic head groups; thus, they show a strong electrostatic screening effect and dehydration of surfactant head groups, whereas the mismatched counterions and ionic head groups, such as kosmotropic counterions Na⁺ and chaotropic head group sulfonate, should remain separated by at least one water molecule, thus showing a weak electrostatic screening effect. Therefore, the strong-binding counterions Br[−]⁶⁴ are efficient in shielding the surface charge of the mixed aggregates with excess CTA⁺. Considering those ATPS-C similar to sample n7, a relatively large amount of Br[−] ions and a relatively large molar ratio between the amounts of Br[−] ions and those of (CTA⁺–AS[−]) imply strong counterion screening of inter- and intra-aggregate electrostatic interactions. The electrostatic screening effect of Na⁺ ions on the mixed aggregates with excess AS[−] is weak, implying that in ATPS-A, similar to sample n5, there is weak counterion screening of inter- and intra-aggregate electrostatic interactions.

The above discussion suggests that electrostatic interactions play a prominent role in setting the type of ATPS. Strong

counterion screening of inter- and intra-aggregate electrostatic interactions arising from strong-binding counterions or a large molar ratio between counterions and their corresponding surfactant ions is beneficial for the formation of the first kind of ATPS, whereas weak counterion screening of inter- and intra-aggregate electrostatic interactions arising from weak-binding counterions or a small molar ratio between counterions and their corresponding surfactant ions is beneficial for the formation of the second kind of ATPS.

4.3. Properties of the Separated Phases in ATPS.

In order to know much more about the two kinds of ATPS, phase shear viscosities, densities, and interfacial tensions of the 11 chosen ATPS samples have been investigated. Figure 4 presents the variation of shear viscosities of the separated phases in these ATPS samples with shear time under constant shear rates. The two kinds of ATPS show different rheological behaviors. It is worthwhile to note that all of the bottom phases in the first kind of ATPS are Newtonian fluids and have low viscosities close to that of water.

The results in Figure 4A and Figure 5 illustrate that for the first kind of ATPS, whether the top phases are isotropic or birefringent, the concentrated top phases are non-Newtonian fluids with not large viscosities (usually about 10–100 mPa·s). Meanwhile, the shear viscosities of these top phases are dependent on shear time as well as the shear rate. The same top phase may show different rheological behaviors under different shear rates, but all show shear-thinning behaviors. These results suggest that for these top phases, the rate of microstructure breakdown under constant shear rate is unequal to the rate of microstructure rebuilding.

The results in Figure 4B indicate that for the second kind of ATPS, both the top phases and their corresponding bottom phases are non-Newtonian fluids and have significantly different viscosities (usually several to several hundred mPa·s) with water. For those ATPSs with a birefringent top phase and isotropic bottom phase (such as n5 and n8–n11), because of the remarkable time-thickening (antithixotropic) behavior of the concentrated birefringent phase,⁶⁵ under constant shear rate, the viscosity of the top phase is usually smaller and then larger than that of the corresponding bottom phase as the shear

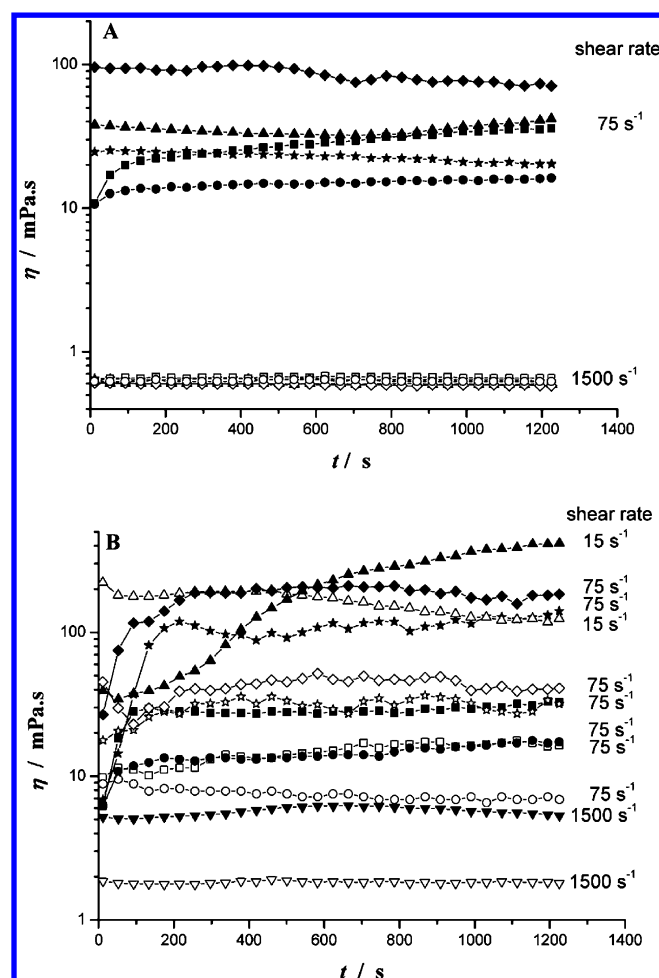


Figure 4. Shear viscosity versus shear time for the separated phases in ATPS under constant shear rates. (A) ★ and ☆: sample *n*1; ■ and □: *n*2; ▲ and △: *n*3; ◆ and ◇: *n*4; ● and ○: *n*7. (B) ● and ○: *n*5; ▼ and ▽: *n*6; ■ and □: *n*8; ★ and ☆: *n*9; ▲ and △: *n*10; ◆ and ◇: *n*11. Closed symbols: top phase; open symbols: bottom phase.

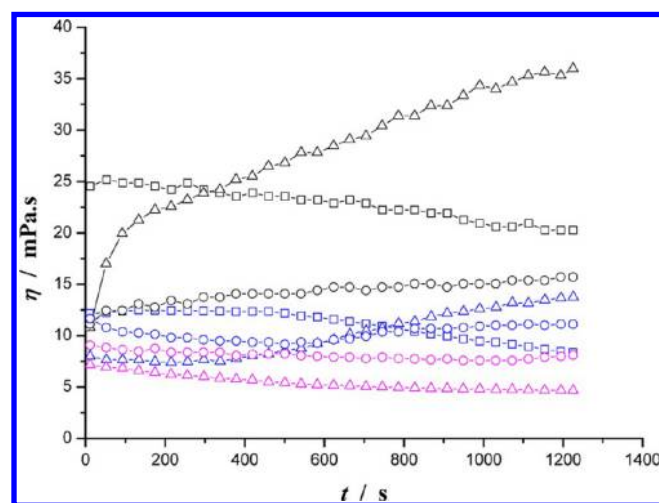


Figure 5. Shear viscosity versus shear time for the top phases in ATPS under constant shear rates. sample *n*1: black □ shear rate 75 s⁻¹, blue □ 1500 s⁻¹; sample *n*2: black △ shear rate 75 s⁻¹, blue △ 75 s⁻¹, pink △ 1500 s⁻¹; sample *n*7: black ○ shear rate 75 s⁻¹, blue ○ 225 s⁻¹, pink ○ 375 s⁻¹.

time is short and then long, respectively. For the ATPS with an isotropic top phase and birefringent bottom phase, the viscosity of the top phase is larger than that of the bottom phase.

Table 2 gives the phase densities and interfacial tensions of the 11 ATPS samples. ρ_T and ρ_B represent the density of the

Table 2. Phase Densities and Interfacial Tensions of ATPS

| sample | $\rho_T/\text{g}\cdot\text{cm}^{-3}$ | $\rho_B/\text{g}\cdot\text{cm}^{-3}$ | $\sigma/\mu\text{N}\cdot\text{m}^{-1}$ |
|-------------|--------------------------------------|--------------------------------------|--|
| <i>n</i> 1 | 0.99978 | 1.00109 | 0.896 |
| <i>n</i> 2 | 0.99889 | 1.00179 | 0.902 |
| <i>n</i> 3 | 0.99554 | 1.00102 | 0.581 |
| <i>n</i> 4 | 0.99694 | 1.00033 | 1.542 |
| <i>n</i> 5 | 0.99222 | 0.99240 | |
| <i>n</i> 6 | 0.99092 | 0.99193 | |
| <i>n</i> 7 | 0.99103 | 0.99270 | 1.350 |
| <i>n</i> 8 | 0.99127 | 0.99214 | 0.256 |
| <i>n</i> 9 | 0.98956 | 0.99178 | 2.364 |
| <i>n</i> 10 | 0.98494 | 0.98909 | 4.030 |
| <i>n</i> 11 | 0.98541 | 0.98816 | 1.420 |

top phase and the density of the bottom phase, respectively. σ represents the interfacial tension of ATPS. The results illustrate that the densities of the separated phases in one ATPS are very close to each other (with differences of about several tenths to several $\text{mg}\cdot\text{cm}^{-3}$). Interfacial tension experimental results indicate that σ between the top phase and the bottom phase of one ATPS is ultralow (several tenths to several $\mu\text{N}\cdot\text{m}^{-1}$). However, for samples *n*5 and *n*6, similar to our previous work,⁵⁰ σ cannot be measured by the spinning drop method due to the fact that both the density difference and the composition difference between coexisting phases are very small. On the basis of the previous work, we can reasonably speculate that σ in *n*5 or *n*6 should be smaller. The combination of an all-aqueous environment and the very low interfacial tension makes these ATPSs ideal for purification and extraction of active biological materials.⁶⁶

4.4. Microstructures of the Separated Phases in ATPS.

The rheological properties of fluids are greatly affected by their microstructures. Composition analysis, property investigation, as well as the microstructure observations may provide important information to reveal the phase separation mechanism. For the first kind of ATPS, the TEM micrographs in Figure 6 reveal that spherical micelles (Figure 6B, D, and F) form in these bottom phases, which is why these bottom phases are Newtonian fluids and have low viscosities close to that of water. Cryo-TEM images reveal that entangled rod-like micelles (Figure 6A and E) form in the isotropic top phases of the first kind of ATPS. Polarization photograph (Figure 6C) illustrates that the birefringent top phase of sample *n*2 is a lamellar crystalline phase.

For the second kind of ATPS, one birefringent phase coexists with one isotropic phase. The polarization photographs (Figure S1, Supporting Information) and cryo-TEM images (Figure 6A, C, and E) illustrate that these birefringent phases are lamellar crystals typified by stacked vesicles and lamellae with large sizes. Weak birefringence was observed in the vesicle top phase of sample *n*5. Birefringence becomes gradually stronger from the vesicle top phase to the stacked lamellae one and then to the densely stacked lamellae one for samples *n*5, *n*8, and *n*10, respectively. Meanwhile, the increase in the compactness of the microstructure in Figure 7 for these top phases leads to the increase of viscosity. Cryo-TEM images in Figure 7B, D, and F

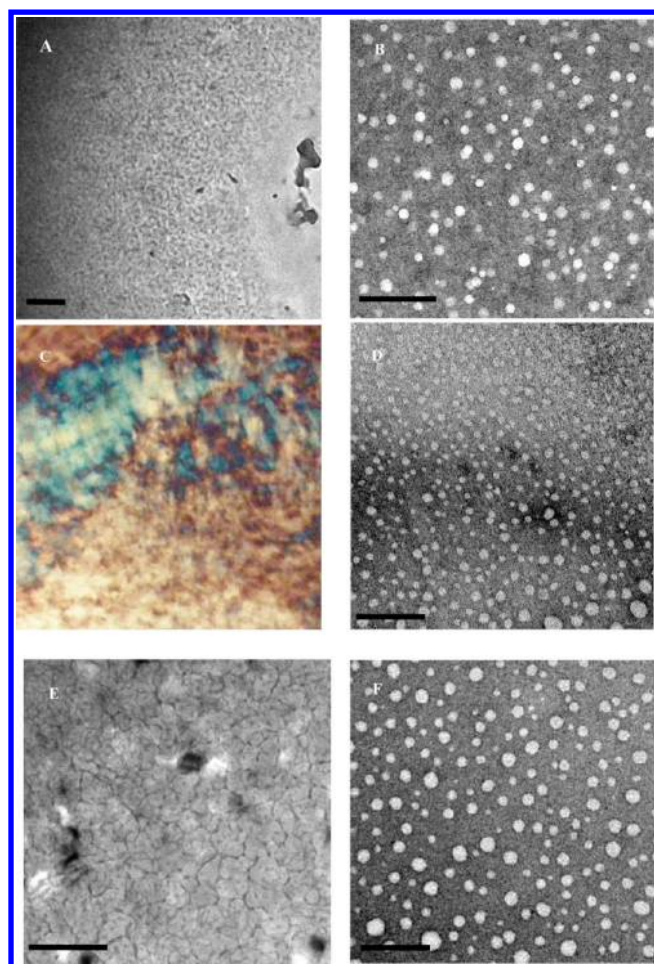


Figure 6. Polarization photograph and TEM micrographs of the separated phases in the first kind of ATPS. (A,E) Cryo-TEM; (B,D,F) negatively stained TEM; (C) polarizing microscope. (A,B) Top phase and bottom phase of sample *n*1, respectively; (C,D) top phase (100-fold) and bottom phase of sample *n*3, respectively; (E,F) top phase and bottom phase of sample *n*4, respectively; scale bar = 200 nm.

illustrate that rod-like micelles form in the isotropic bottom phases of this kind of ATPS. That is why these bottom phases have obvious different viscosities than water.

The above TEM images reveal that for the CTAB–AS–CTA⁺AS[−]–NaBr–H₂O system, aqueous two-phase separation is closely related to entanglement of rod-like micelles, or the formation of a lamellar phase, or the formation of densely packed vesicles. According to the geometric model,^{63,67–69} the overall packing shape of surfactant molecules can be conveniently described by the dimensionless critical packing parameter $p = v/(l_{\max} a)$, where v and l_{\max} are the volume and length of the hydrophobic chain, respectively, and a is the apparent area per molecule at the interface (hydrated head group). Rod-like micelles are expected in the range of $1/3 < p < 1/2$, vesicles are expected in the range of $1/2 < p < 1$, and lamellar aggregates are expected for p close to 1. The above information suggests that the formation of ATPS is favorable at a certain p range. For ATPS-A or ATPS-C, the mixed aggregates are negatively or positively charged, respectively. The increase of counterions under certain x_T is favored for the counterion binding with the oppositely charged aggregates, thus reducing a , whereas it does not significantly influence v and l_{\max} and consequently increases the p value. To maintain the p

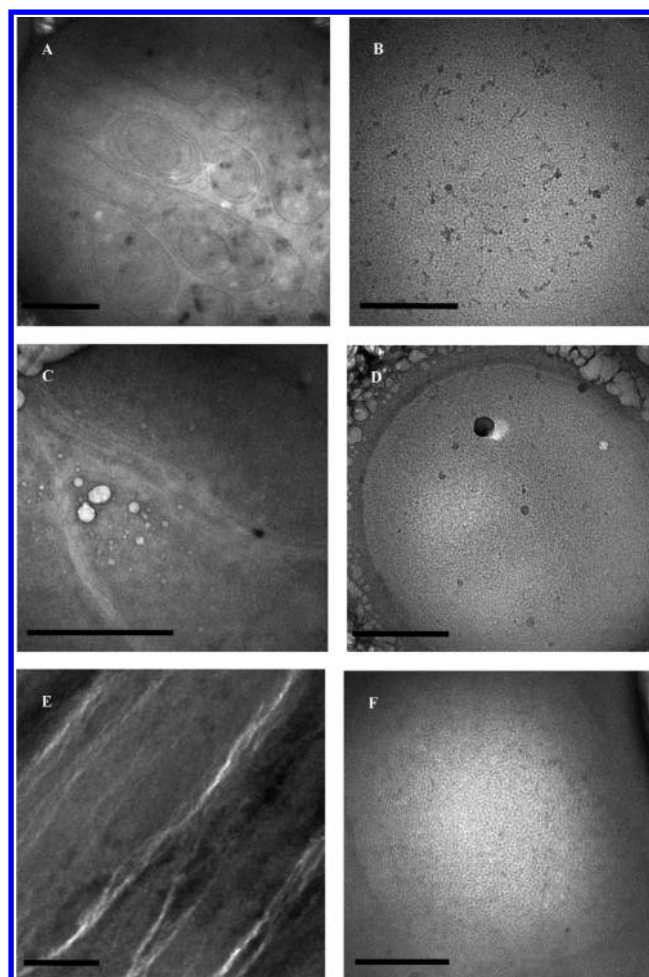


Figure 7. Cryo-TEM micrographs of the separated phases in the second kind of ATPS. (A,B) Top phase and bottom phase of sample *n*5, respectively; (C,D) top phase and bottom phase of sample *n*8, respectively; (E,F) top phase and bottom phase of sample *n*10, respectively; scale bars = 500 nm.

range, the ATPS-A region shifts to the higher MR_{AS^-/CTA^+} side, and the ATPS-C region shifts to the higher MR_{CTA^+/AS^-} side.

In order to understand the aqueous two-phase separation process more deeply, two samples were chosen for further investigation. Sample *n*12 (the whole sample prepared: $x_{CTA^+} = 0.552 \times 10^{-3}$, $x_{AS^-} = 1.262 \times 10^{-3}$, $x_{Br^-} = 2.347 \times 10^{-3}$, and $x_{Na^+} = 3.058 \times 10^{-3}$) is similar to sample *n*1, belongs to the first kind of ATPS, but has longer aqueous two-phase separation time (sample *n*12 or *n*1: about 105 or 6 min, respectively). Sample *n*5 belongs to the second kind of ATPS whose aqueous two-phase separation time is about 90 min. Figure 8 gives the cryo-TEM images of samples *n*12 and *n*5 in the process of self-assembly after the two oppositely charged surfactant stock solutions were mixed and before the aqueous two-phase separated. Cryo-TEM images illustrate that in the formation process of ATPS, rod-like micelles coexist with spherical micelles in sample *n*12; vesicles coexist with rod-like micelles in sample *n*5. For sample *n*12, the entanglement of rod-like micelles leads to phase separation, and the spherical micelles were left in the dilute phase. For sample *n*5, large vesicles form by the fusion of smaller vesicles, and then, the densely packed large vesicles induce phase separation, whereas the rod-like micelles are left in the dilute phase.

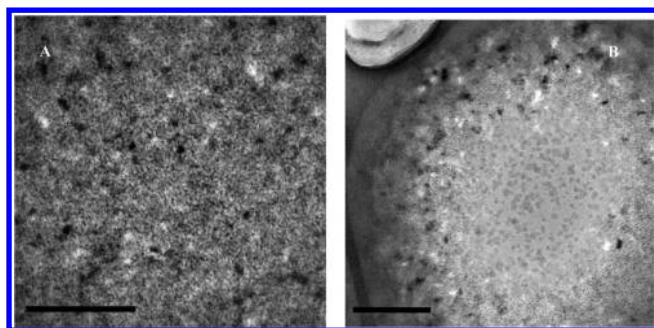


Figure 8. Cryo-TEM micrographs of samples *n*12 and *n*5 in the formation process of ATPS. (A) Sample *n*12, 50 min after the two surfactant stock solutions were mixed; (B) sample *n*5, 30 min after the two surfactant stock solutions were mixed; scale bars = 500 nm.

4.5. Aqueous Two-Phase Separation Modes. The composition analysis, property investigations, and TEM images illustrate that there are two different kinds of ATPSs dependent on the counterion binding effect. According to Coulomb's law, oppositely charged ions attract each other, like-charged ions repel each other. For the mixed systems at the NaBr side of the pyramid, high molar ratios between the counterions and their corresponding surfactant ions indicate strong counterion binding with the charged aggregates and strong electrostatic screening the repulsion between the like-charged head groups, and thus, the formation of aggregates with the bulk composition becomes possible. According to Kaler's thermodynamic cell model,^{2,42,43} of all of the contributions to the total free energy of aggregation, only the electrostatic free energy G_{el} (similar to eq 6) is sensitive to the changing of the molar ratio between the counterions and their corresponding surfactant ions. In the first kind of ATPS-A or ATPS-C, aggregates with the bulk composition are obviously negatively or positively charged, and strong counterion binding with the charged aggregates can partially neutralize the surface charge, decrease the surface potential of aggregates ψ_s , and suppress the electrical double layer, thus reducing G_{el} of aggregates effectively. From the viewpoint of thermodynamics, the formation of aggregates with bulk composition in the first kind of ATPS is favorable due to the high counterion binding. The attractions and repulsions between aggregates have enormous significance in the stability of aggregates and the micellization of the surfactant.^{70–74} Some of the most important forces are the van der Waals force, electrostatic double-layer force, hydration force,^{72–74} and steric force. The first two are long-range forces, and the last two are the most remarkable short-range forces. For the ionic surfactant aggregates, the repulsive electrostatic double-layer, hydration, and steric forces counteract the attractive van der Waals force to prevent the coagulation of aggregates. Because the high counterion binding with charged aggregates effectively shields the interaggregate electrostatic repulsion⁴⁵ and leads to dehydration of the surfactant head groups and bound counterions, there is less hydration repulsion.⁷² The van der Waals attraction decreases at increasing electrolyte concentration, but it does not decrease as much as the repulsions.⁷² Therefore, the effect of the van der Waals attractions between aggregates becomes significant and triumphs over that of repulsions,^{45,72} and the coagulation of the aggregates with the bulk composition is promoted, thus leading to phase separation.^{46,72} That is, electrostatic interactions between the oppositely charged head groups, between the like-charged head

groups in excess, as well as between the like-charged aggregates in the first kind of ATPS are beneficial for the formation of aggregates with the bulk composition and their coagulation due to strong electrostatic screening of counterions, thus leading to the first kind of aqueous two-phase separation. In the meantime, small spherical micelles (Figure 8A) form due to electrostatic attraction between a small amount of free monomeric CTA^+ and AS^- ions dispersed in medium and low CMC values (several dozens of $\mu\text{mol}\cdot\text{kg}^{-1}$) of the mixed systems, and the formed spherical micelles are left in the dilute phase (Figure 6). That is why these bottom phases are very dilute in surfactant ions and low viscous Newtonian fluids, and the concentration difference of the surfactant ions between the top phase and the bottom phase is large. Therefore, the first kind of ATPSs are potential extraction systems.

For the CTAB-AS- CTA^+AS^- -NaBr- H_2O system at the CTA^+AS^- side of the pyramid, the molar ratios between the counterions and their corresponding surfactant ions are low, if the composition of the aggregates formed in ATPS-A or ATPS-C equals that of the bulk composition, and low counterion binding to these negatively or positively charged aggregates means high surface charge density, high ψ_s , and a thick double layer, thus leading to a high G_{el} of aggregation. From the viewpoint of thermodynamics, as a result of weak electrostatic screening of counterions, the strong electrostatic attraction between CTA^+ and AS^- head groups leads to the formation of more neutral aggregates rather than aggregates with the bulk composition, and the charge neutralization at the level of the head groups thus reduces the surface charge of the aggregates, ψ_s , and the double-layer thickness. Therefore, the formation of aggregates with a more neutral composition than the bulk composition leads to a small electrostatic free energy G_{el} . The effective area per ionic head group in these aggregates decreases due to stronger electrostatic attraction between oppositely charged CTA^+ and AS^- head groups, thus increasing the critical packing parameter.⁷⁵ It means that vesicles or lamellae are easy to form. Meanwhile, the charge neutralization between the oppositely charged head groups releases some of the constituent counterions of surfactants to the remaining bulk solution; then, in the remaining system, the formation of aggregates with a composition far away from equimolar is favorable due to a stronger counterion binding ability. Higher counterion binding with the charged aggregates reduces G_{el} of aggregation to some extent due to partially neutralizing the surface charge, decreasing ψ_s , and suppressing the electrical double layer. The composition and counterion binding degree determine that it is conducive to form rod-like aggregates in the remaining system (Figure 8B). That is, in the second kind of ATPS, two different kinds of large aggregates are in favor of forming, one (vesicle or lamella) with more neutral composition (Figure 7A, C, and E) and lower counterion binding and the other (rod-like aggregate) with a composition farther from equimolar (Figure 7B, D, and F) and a higher counterion binding; their formation leads to lower G_{el} than the formation of aggregates with bulk composition. For the preferentially formed vesicles or lamellae with more neutral composition, weaker interaggregate electrostatic repulsion and hydration repulsion means the strengthening of the interaggregate attraction; therefore, it is beneficial for the lamellar phase separation from the system due to the dense stack of the vesicles or lamellae. Correspondingly, the rod-like aggregates were left in the dilute phase of ATPS. Because both kinds of aggregates with different microstructures have strong forming

tendency, the concentration difference of surfactant ions between the top phase and bottom phase is not large. Under certain conditions, in comparison with the ATPS with the same x_T in the conventional mixing plane, the more easily formed lamellar liquid-crystalline phase has a larger concentration difference with the dilute bottom phase in ATPS at the CTA^+AS^- side of the pyramid; therefore, ATPSs analogous to samples *n*8 and *n*9 are also potential extraction systems. The situation of ATPS in the CTA^+AS^- – AS – H_2O side plane and the CTA^+AS^- – CTAB – H_2O side plane is analogous.

5. CONCLUSIONS

In this paper, the systematic investigation of the CTAB – AS – CTA^+AS^- – NaBr – H_2O system illustrates that the molar ratio between the counterions and their corresponding surfactant ions is a crucial factor influencing the aqueous two-phase separation. The variation of the molar ratio not only influences the extension of aqueous two-phase regions in the three-dimensional space of the pyramid phase diagram but also influences the phase separation modes, compositions, properties, and microstructures of ATPS.

The molar ratio between the counterions and their corresponding surfactant ions is one important factor influencing the electrostatic screening effect of counterions, thus playing a key role in tuning the electrostatic interaction between the ionic head groups and that between the charged aggregates, and then affects the aqueous two-phase behaviors. On the basis of Kaler's cell model, a high molar ratio between counterions and the surfactant ions or a strong-binding inorganic counterion is beneficial for the formation of aggregates with the bulk composition that correspond to low G_{el} and the strong electrostatic screening of the interaggregate electrostatic repulsion is in favor of the coagulation of aggregates, thus leading to the first kind of aqueous two-phase separation. A low molar ratio between counterions and the surfactant ions or weak-binding inorganic counterion is beneficial for the formation of two different kinds of aggregates, a vesicle or lamella with more neutral composition and lower counterion binding and a rod-like aggregate with more a far from equimolar composition and higher counterion binding, which correspond to lower G_{el} than the formation of aggregates with the bulk composition; weak interaggregate electrostatic repulsion is in favor of a dense stack of the vesicles or lamellae with more neutral composition, thus leading to the second kind of aqueous two-phase separation.

This investigation provides a possible means to tune the aqueous two-phase behaviors and the properties of the oppositely charged surfactant systems. This control is important for the further understanding of the phase separation mechanism of ATPS and for the potential applications of ATPSs to biotechnology separation, industrial separations, and waste remediations. Furthermore, the systematic investigation of phase compositions, phase densities, interfacial tensions, and rheological properties of ATPS provides fundamental data for the development of the corresponding theoretical model and the design of extraction equipment.

■ ASSOCIATED CONTENT

Supporting Information

Polarization photographs of the top phases in the second kind of ATPS. This material is available free of charge via the Internet at <http://pubs.acs.org>.

■ AUTHOR INFORMATION

Corresponding Author

*Tel: +86-731-88872530. Fax: +86-731-88872531. E-mail: nanyq@qq.com.

Notes

The authors declare no competing financial interest.

■ ACKNOWLEDGMENTS

We gratefully acknowledge the National Natural Science Foundation of China (21076069 and 20976042) and Hunan Provincial Natural Science Foundation of China (09JJ1001) for financial support of this project. The authors gratefully acknowledge Professor Jing-Cheng Hao for his help; the cryo-TEM experiments were performed by Professor Jing-Cheng Hao's group.

■ REFERENCES

- (1) Lucassen-Reynders, E. H.; Lucassen, J.; Giles, D. J. *Colloid Interface Sci.* **1981**, *81*, 150–157.
- (2) Herrington, K. L.; Kaler, E. W.; Miller, D. D.; Zasadzinski, J. A.; Chiruvolu, S. J. *Phys. Chem.* **1993**, *97*, 13792–13802.
- (3) Zana, R.; Lvy, H.; Danino, D.; Talmon, Y.; Kwetkat, K. *Langmuir* **1997**, *13*, 402–408.
- (4) Sohrabi, B.; Gharibi, H.; Tajik, B.; Javadian, S.; Hashemianzadeh, M. J. *Phys. Chem. B* **2008**, *112*, 14869–14876.
- (5) Liu, L.; Rosen, M. J. *Colloid Interface Sci.* **1996**, *179*, 454–459.
- (6) Vivares, D.; Soussan, E.; Blanzat, M.; Rico-Lattes, I. *Langmuir* **2008**, *24*, 9260–9267.
- (7) Renoncourt, A.; Vlachy, N.; Bauduin, P.; Drechsler, M.; Touraud, D.; Verbavatz, J.-M.; Dubois, M.; Kunz, W.; Ninham, B. W. *Langmuir* **2007**, *23*, 2376–2381.
- (8) Kaler, E. W.; Murthy, K. A.; Rodriguez, B. E.; Zasadzinski, J. A. N. *Science* **1989**, *245*, 1371–1374.
- (9) Dubois, M.; Demé, B.; Gulik-Krzywicki, Th.; Dediu, J. C.; Vautrin, C.; Désert, S.; Perez, E.; Zemb, Th. *Nature* **2001**, *411*, 672–675.
- (10) Zemb, Th.; Dubois, M.; Demé, B.; Gulik-Krzywicki, Th. *Science* **1999**, *283*, 816–819.
- (11) Bergström, M.; Pederson, J. S. *Langmuir* **1999**, *15*, 2250–2253.
- (12) Hao, J.; Hoffmann, H. *Curr. Opin. Colloid Interface Sci.* **2004**, *9*, 279–293.
- (13) Koehler, R. D.; Raghavan, S. R.; Kaler, E. W. *J. Phys. Chem. B* **2000**, *104*, 11035–11044.
- (14) Ziserman, L.; Abezgauz, L.; Ramon, O.; Raghavan, S. R.; Danino, D. *Langmuir* **2009**, *25*, 10483–10489.
- (15) Rosa, M.; Infante, M. R.; Miguel, M.; da, G.; Lindman, B. *Langmuir* **2006**, *22*, 5588–5596.
- (16) Dong, S.; Song, A.; Hao, J. *Colloids Surf., A* **2010**, *359*, 53–59.
- (17) Tsuchiya, K.; Ishikake, J.; Kim, T. S.; Ohkubo, T.; Sakai, H.; Abe, M. J. *Colloid Interface Sci.* **2007**, *312*, 139–145.
- (18) Kaler, E. W.; Herrington, K. L.; Murthy, A. K.; Zasadzinski, J. A. N. *J. Phys. Chem.* **1992**, *96*, 6698–6707.
- (19) Marquez, E. F.; Oren, R.; Khan, A.; Miguel, M.; Lindman, B. J. *Phys. Chem.* **1998**, *102*, 6746–6758.
- (20) Sjöbom, M. B.; Edlund, H. *Langmuir* **2002**, *18*, 8309–8317.
- (21) Ogura, T.; Sakai, K.; Sakai, H.; Abe, M. J. *Phys. Chem. C* **2008**, *112*, 12184–12187.
- (22) Zhao, N.; Wei, Y.; Sun, N.; Chen, Q.; Bai, J.; Zhou, L.; Qin, Y.; Li, M.; Qi, L. *Langmuir* **2008**, *24*, 991–998.
- (23) McKelvey, C. A.; Kaler, E. W.; Zasadzinski, J. A.; Coldren, B.; Jung, H.-T. *Langmuir* **2000**, *16*, 8285–8290.
- (24) Hentze, H.-P.; Raghavan, S. R.; McKelvey, C. A.; Kaler, E. W. *Langmuir* **2003**, *19*, 1069–1074.
- (25) Chen, F.; Huang, L.; Li, Q. *Chem. Mater.* **1997**, *9*, 2685–2686.
- (26) Pevzner, S.; Regev, O.; Lind, A.; Lindén, M. J. *Am. Chem. Soc.* **2003**, *125*, 652–653.
- (27) Zhao, N.; Qi, L. *Adv. Mater.* **2006**, *18*, 359–362.

- (28) Dong, R.; Weng, R.; Dou, Y.; Zhang, L.; Hao, J. *J. Phys. Chem. B* **2010**, *114*, 2131–2139.
- (29) Zhang, H.; Li, H.; Li, D.; Meng, S. *J. Colloid Interface Sci.* **2006**, *302*, 509–515.
- (30) Akama, Y.; Tong, A.; Ito, M.; Tanaka, S. *Talanta* **1999**, *48*, 1133–1137.
- (31) Xiao, J.-X.; Sivars, U.; Tjerneld, F. *J. Chromatogr., B* **2000**, *743*, 327–338.
- (32) Nan, Y.; Hao, L.; Liu, H.; Hu, Y. *J. Dispersion Sci. Technol.* **2006**, *27*, 419–425.
- (33) Wang, K.; Yin, H.; Sha, W.; Huang, J.; Fu, H. *J. Phys. Chem. B* **2007**, *111*, 12997–13005.
- (34) Weschayanwivat, P.; Kunanupap, O.; Scamehorn, J. F. *Chemosphere* **2008**, *72*, 1043–1048.
- (35) Zhao, G.-X.; Xiao, J.-X. *J. Colloid Interface Sci.* **1996**, *177*, 513–518.
- (36) Jiang, R.; Huang, Y.-X.; Zhao, J.-X.; Huang, C.-C. *Fluid Phase Equilib.* **2009**, *277*, 114–120.
- (37) Lu, T.; Li, Z.; Huang, J.; Fu, H. *Langmuir* **2008**, *24*, 10723–10728.
- (38) Shang, Y.; Liu, H.; Hu, Y.; Prausnitz, J. M. *Colloids Surf., A* **2007**, *302*, 58–66.
- (39) Nan, Y.-Q.; Hao, L.-S. *J. Phys. Chem. B* **2008**, *112*, 12326–12337.
- (40) Nan, Y.; Liu, H.; Hu, Y. *Colloids Surf., A* **2005**, *269*, 101–111.
- (41) Nan, Y.; Liu, H.; Hu, Y. *Colloids Surf., A* **2006**, *277*, 230–238.
- (42) Brasher, L. L.; Herrington, K. L.; Kaler, E. W. *Langmuir* **1995**, *11*, 4267–4277.
- (43) Brasher, L. L.; Kaler, E. W. *Langmuir* **1996**, *12*, 6270–6276.
- (44) Yuet, P. K.; Blankschtein, D. *Langmuir* **1996**, *12*, 3802–3818.
- (45) Vlachy, N.; Renoncourt, A.; Drechsler, M.; Verbavatz, J.-M.; Touraud, D.; Kunz, W. *J. Colloid Interface Sci.* **2008**, *320*, 360–363.
- (46) Hao, L.-S.; Nan, Y.-Q. *Colloids Surf., A* **2008**, *325*, 186–193.
- (47) Marques, E.; Khan, A.; Miguel, M. G.; Lindman, B. *J. Phys. Chem.* **1993**, *97*, 4729–4736.
- (48) Thalberg, K.; Lindman, B.; Karlström, G. *J. Phys. Chem.* **1991**, *95*, 6004–6011.
- (49) Zhu, B.; Zhang, P.; Huang, J.; Zhao, G. *Acta Phys. Chim. Sin.* **1999**, *15*, 110–115.
- (50) Nan, Y.-Q.; Liu, H.-L.; Hu, Y. *J. Colloid Interface Sci.* **2006**, *293*, 464–474.
- (51) Wang, P.; Anderko, A. *Fluid Phase Equilib.* **2001**, *186*, 103–122.
- (52) Szleifer, I.; Ben-Shaul, A.; Gelbart, W. M. *J. Chem. Phys.* **1985**, *83*, 3612–3620.
- (53) Szleifer, I.; Kramer, D.; Ben-Shaul, A.; Gelbart, W. M.; Safran, S. A. *J. Chem. Phys.* **1990**, *92*, 6800–6817.
- (54) Jokela, P.; Jönsson, B.; Khan, A. *J. Phys. Chem.* **1987**, *91*, 3291–3298.
- (55) Marques, E. F.; Brito, R. O.; Wang, Y.; Silva, B. F. B. *J. Colloid Interface Sci.* **2006**, *294*, 240–247.
- (56) Vlachy, N.; Arteaga, A. F.; Klaus, A.; Touraud, D.; Drechsler, M.; Kunz, W. *Colloids Surf., A* **2009**, *338*, 135–141.
- (57) Hao, L.-S.; Deng, Y.-T.; Zhou, L.-S.; Ye, H.; Nan, Y.-Q.; Hu, P. *J. Phys. Chem. B* **2012**, *116*, 5213–5225.
- (58) You, Y.-L.; Hao, L.-S.; Nan, Y.-Q. *Colloids Surf., A* **2009**, *335*, 154–167.
- (59) Ilekli, P.; Piculell, L.; Tournilhac, F.; Cabane, B. *J. Phys. Chem. B* **1998**, *102*, 344–351.
- (60) Ilekli, P.; Martin, T.; Cabane, B.; Piculell, L. *J. Phys. Chem. B* **1999**, *103*, 9831–9840.
- (61) Pi, Y.; Shang, Y.; Peng, C.; Liu, H.; Hu, Y.; Jiang, J. *J. Colloid Interface Sci.* **2006**, *299*, 410–415.
- (62) Collins, K. D. *Methods* **2004**, *34*, 300–311.
- (63) Vlachy, N.; Jagoda-Cwiklik, B.; Vácha, R.; Touraud, D.; Jungwirth, P.; Kunz, W. *Adv. Colloid Interface Sci.* **2009**, *146*, 42–47.
- (64) Ge, W.; Shi, H.; Talmon, Y.; Hart, D. J.; Zakin, J. L. *J. Phys. Chem. B* **2011**, *115*, 5939–5946.
- (65) Partal, P.; Kowalski, A. J.; Machin, D.; Kiratzis, N.; Berni, M. G.; Lawrence, C. J. *Langmuir* **2001**, *17*, 1331–1337.
- (66) Ziemecka, I.; Steijn, V.; Koper, Ger. J. M.; Rosso, M.; Brizard, A. M.; Esch, J. H.; Kreutzer, M. T. *Lab Chip* **2011**, *11*, 620–624.
- (67) Tanford, C. *The Hydrophobic Effect*; Wiley: New York, 1980.
- (68) Israelachvili, J. N.; Mitchell, D. J.; Ninham, B. W. *J. Chem. Soc., Faraday Trans. 2* **1976**, *72*, 1525–1568.
- (69) Israelachvili, J. N. *Intermolecular and Surface Forces*; Academic Press: New York, 1985.
- (70) Ghosh, P. *Colloid and Interface Science*; PHI Learning: New Delhi, 2009.
- (71) Israelachvili, J. N. *Intermolecular and Surface Forces*, 3rd ed.; Academic Press: London, 2011.
- (72) Sein, A.; Engberts, J. B. F. N. *Langmuir* **1995**, *11*, 455–465.
- (73) Marčelja, S.; Radić, N. *Chem. Phys. Lett.* **1976**, *42*, 129–130.
- (74) Rand, R. P.; Parsegian, V. A. *Biochim. Biophys. Acta* **1989**, *988*, 351–376.
- (75) Caria, A.; Khan, A. *Langmuir* **1996**, *12*, 6282–6290.